Vision Correcting Displays Based on Inverse Blurring and Aberration Compensation

Brian A. Barsky[1,2(✉)], Fu-Chung Huang[1,4], Douglas Lanman[3,5], Gordon Wetzstein[3], and Ramesh Raskar[3]

[1] Computer Science Division, UC Berkeley, Berkeley, USA
barsky@berkeley.edu
[2] School of Optometry, UC Berkeley, Berkeley, USA
[3] MIT Media Lab, Providence, USA
[4] Microsoft, Berkeley, USA
[5] Oculus VR, Irvine, USA

Abstract. The concept of a vision correcting display involves digitally modifying the content of a display using measurements of the optical aberrations of the viewer's eye so that the display can be seen in sharp focus by the user without requiring the use of eyeglasses or contact lenses. Our first approach inversely blurs the image content on a single layer. After identifying fundamental limitations of this approach, we propose the multilayer concept. We then develop a fractional frequency separation method to enhance the image contrast and build a multilayer prototype comprising transparent LCDs. Finally, we combine our viewer-adaptive inverse blurring with off-the-shelf lenslets or parallax barriers and demonstrate that the resulting vision-correcting computational display system facilitates significantly higher contrast and resolution as compared to previous solutions. We also demonstrate the capability to correct higher order aberrations.

Keywords: Aberrations · Visual correction · Multilayer display · Deconvolution · Transparent LCDs · Light field display

1 Introduction

This work presents an alternative to eyeglasses, contact lenses, and refractive surgeries for addressing the problem of blurred human vision. The idea is to "digitally" modify the content on a display device so that when viewed by a particular user it will appear in sharp focus for this individual. This process comprises both algorithmic operations that are functions of the particular user's optical aberrations and modified display optics at a hardware level that are the same for all users. Once the display device is built, the refractive errors are corrected digitally; no further adjustment to the optical hardware component is required for different users. We correct for myopia or hyperopia and also consider more complicated blur induced by higher order aberrations.

Using an eyeglasses prescription [14] or aberration measurements from a Hartmann-Shack wavefront aberrometer [2,3] to identify the Point Spread

L. Agapito et al. (Eds.): ECCV 2014 Workshops, Part III, LNCS 8927, pp. 524–538, 2015.
DOI: 10.1007/978-3-319-16199-0_37

Function (PSF) of the user's eye, we inversely blur the image content such that when it will be viewed by this individual, it will appear in sharp focus.

Considering the sharp image as the result of the inverse blurred image convolved with the blurring kernel that represents the individuals PSF, the inverse blurred image can be computed by convolving the sharp image with the inverse of the blurring kernel that represents the individuals PSF.

This approach has two fundamental limitations due to the nature of blur kernels. First, blur kernels are usually interspersed with zero frequency responses and this results in some loss of frequencies which introduces some blurring and ringing artifacts in the final perceived image. Second, blur kernels are generally low-pass and consequently the frequency inversion in the prefiltering tends to amplify the higher frequencies creating expanded dynamic range requirements; to be able to show the preprocessed image on a conventional display, an image with very low contrast is produced by applying dynamic range compression to the preprocessed image.

To overcome these limitations requires going beyond using only the two-dimensional sharp image and developing higher dimensional methods. We have developed both a multilayer display that comprises a stack of 2D images as well as a light field based method requiring 4D light rays. We performed the conditioning rank analysis, which we showed is equivalent to the modulation transfer function (MTF) zeros analysis. The rank analysis revealed the design parameters of the hardware, and lightly modified hardware provides enough degrees of freedom to achieve the goal of correcting vision. Physical prototype hardware was built to illustrate these benefits. Our light field prefiltering prototype uses an iPhone 4/ iPod Touch 4, and our experimental results demonstrate that it corrects significant defocus blur.

2 Preliminary Ideas with Deconvolution

Since the Fourier transform is linear, *the modulation transfer function is the unsorted singular values, and therefore the zero-valued spatial frequencies match the zero singular values*. The inverse filter and the Wiener filter are like the pseudo-inverse approximation. Since inverting zero singular values is undefined, similarly, inverting the lost frequencies is undefined and thus some regularization strategies must be applied.

These zero-valued spatial frequencies lead to the first theoretical limitation of ringing artifacts and slight blurriness. *The lost frequencies or singular-values cannot be recovered since the blurring kernel is applied at the last step of the process*; generally, this information loss causes blurriness. The lack of certain frequencies at sharp edges generates some ringing artifacts, as shown in Figure 1.

The second problem with inverting the blurring kernel is the extremely expanded dynamic range. Due to the heavily attenuated frequency responses that are close to zero, their inversions are close to infinity, causing these frequencies to exhibit dominating sinusoidal structures in the spatial domain images, and generating negative and overwhelmingly positive pixel

states; intensity re-normalization is required to show the prefiltered image on the display, but this results in reduced contrast.

Thus, there are two fundamental limitations of the prefiltering method using a traditional display:

– Frequency loss causes slight blurriness and ringing artifacts.
– Expanded dynamic range and negative pixel values require intensity re-normalization which causes reduced contrast.

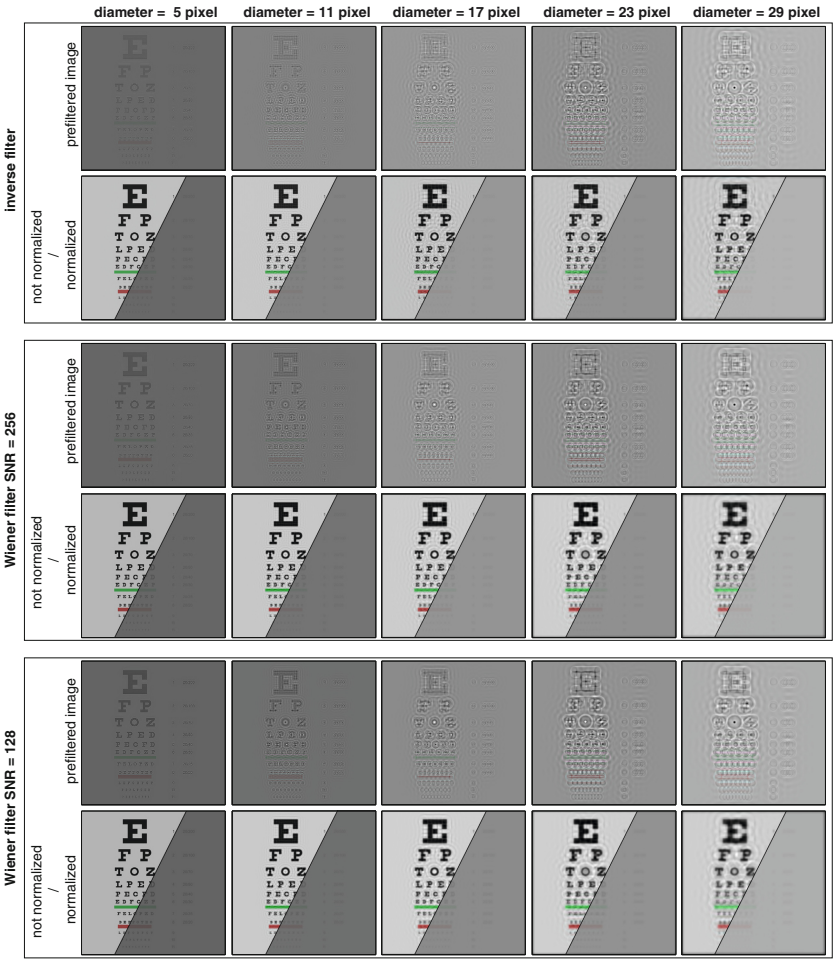

Fig. 1. Frequency domain prefiltering solutions using the inverse filter and the Wiener filter. This type of solvers generally have contrast loss problem. Depending on the regularization, the ringing artifacts can be attenuated and the contrast can be enhanced, but the image can also become more blurry.

Although these drawbacks are lightly documented in the paper by Alonso and Barreto [2], no theoretical improvement has been proposed. With the theoretical

analysis for the prefiltering method on a traditional display, we conclude that the traditional display should be modified and new hardware should be built. In the next section, we will introduce the prefiltering method with a "multilayer" type of display that addresses the fundamental limitations.

3 Multilayer Displays

In this section, we develop inverse prefiltering for emerging multilayer displays. Following the limitations on image prefiltering using the conventional display, as discussed in the previous sections, the multilayer display enables an "all-pass kernel": there will be no zero-valued frequency responses [5]. We will first discuss the observations and intuitions behind the idea, and then develop the theory of multilayer prefiltering [6]; a contrast optimization will be introduced, and finally we will discuss the hardware design alternatives and our prototypes.

3.1 Frequency Preservation via Multilayer Prefiltering

For the case of image prefiltering using a conventional display, we will now refer to the case where only one display panel is used as "single-layer prefiltering." The point spread function is a *disk* function of diameter r and of the distance from the eye to the plane of focus. The closer the display is to the plane of focus, the smaller the point spread function is. This is shown on the left side of Figure 2 which illustrates two cases of defocus blur: Depicted in blue is the display closer to the plane of focus and the resulting smaller point spread function, and shown in green is the display farther from the plane of focus and the resulting larger point spread function.

On the right of Figure 2, we plot the modulation transfer functions (MTFs) of the two PSFs. Since their MTFs are both *jinc* functions with periods determined by the diameter of their PSFs, they both inevitably have the zero-valued problem.

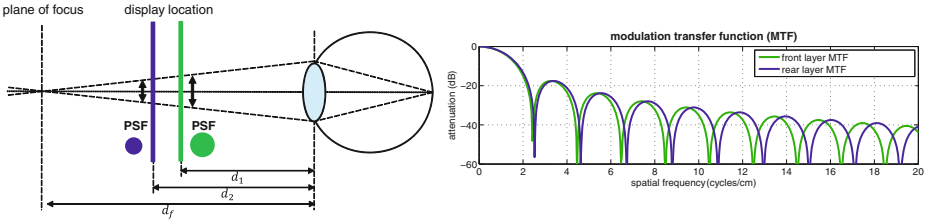

Fig. 2. Observation of multilayer PSFs and their MTFs

However, an important observation is that these zero-valued frequencies generally do not align. By using a carefully chosen separation between the two layers, the coincident frequency will not happen within human perceivable frequencies

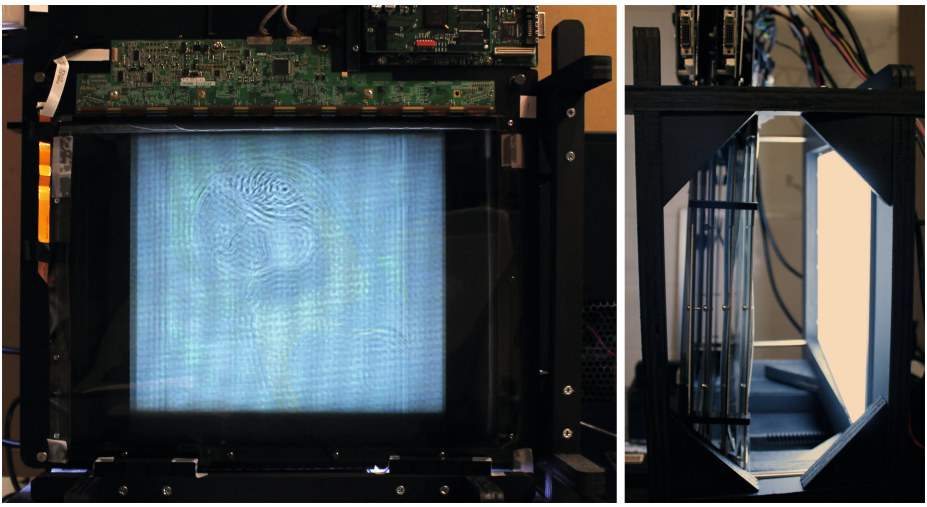

Fig. 3. Prototype multilayer display, front view and side view

(around 60 cycles per degree). This raises the engineering question of how to make both layers visible to the eye and have the two layers still maintain the properties of two different point spread functions. Fortunately, nowadays there are transparent display panels, and they are capable of refreshing at high speed (120Hz panel are commercially available). By utilizing the critical flickering rate (around 40Hz) limiting the temporal integration of the eye, we quickly interchange contents on the two displays, and the eye will fuse the two images on the retina; this is the fundamental idea of our multilayer inverse prefiltering.

3.2 Building a Multilayer Display

Any practical multilayer display must meet four design criteria. It should: (1) be optically equivalent to a stack of semi-transparent, light-emitting layers, (2) be thin, (3) support binocular correction, since refractive errors may differ between eyes, and (4) support a wide field of view. In addition, the display should ideally support HDR modes, due to the expansion in dynamic range. We observe that most of these constraints are shared by autostereoscopic displays. Such displays can be constructed using a wide variety of component technologies, including transparent organic light-emitting diodes (TOLEDs), beam-splitter trees, and liquid-crystal displays (LCDs).

We built an early prototype using a beam-splitter tree, similar to the construction by Akeley et al. [1]: viewing multiple LCDs through a set of half-silvered mirrors (i.e., beam splitters) is optically equivalent to a stack of semi-transparent, light-emitting layers. However, the form factor and field of view of this prototype was not satisfying.

A more practical construction using multilayer LCDs employing the design of Lanman et al. [10] is shown in Figure 3. This prototype comprises four modified 40.8cm-by-30.6cm Barco E-2320 PA LCD panels, supporting 8-bit grayscale display with a resolution of 1600-by-1200 pixels and a refresh rate of 60 Hz. The stack is operated in a time-multiplexed manner such that only one panel displays content at any given time. With a sufficiently long exposure (i.e., $\geq N/60$ seconds when N layers are used), the prototype appears as a semitransparent stack of light-emitting layers.

We record color images by simulating a field sequential color (FSC) backlight (i.e., a strobed backlight that illuminates the stack with time-varying color sources); for the results in Figure 6, we combine three separate photographs, each recorded while displaying a different color channel of the prefiltered images.

3.3 Experimental Results with Multilayer Display

Simulated results. We first show some simulated corrections using both single-layer prefiltering and two-layer prefiltering. The results shown in Figure 4 are

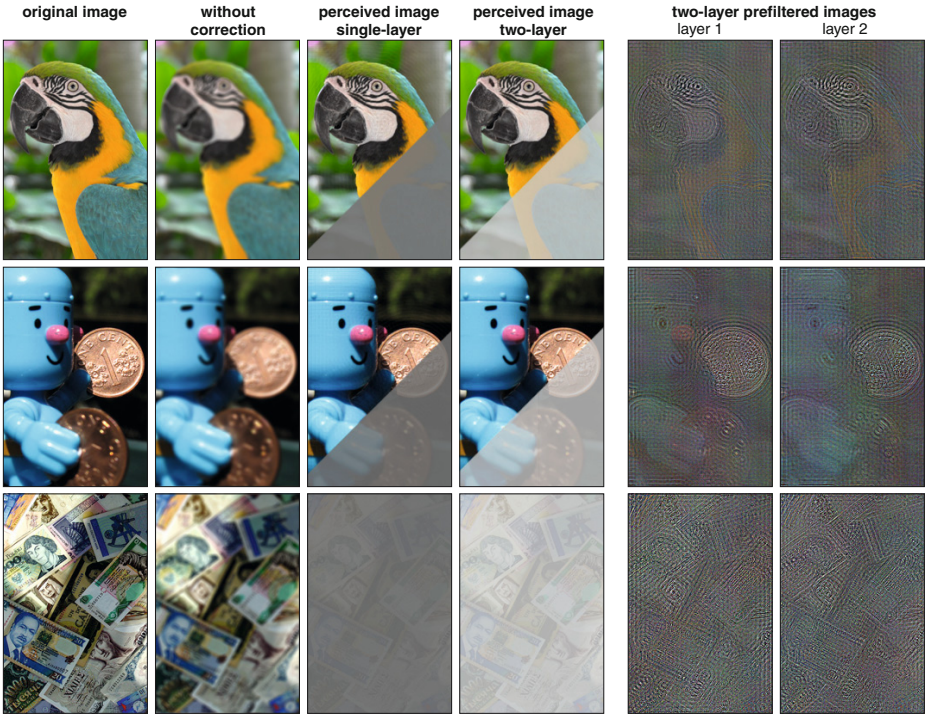

Fig. 4. Comparing simulated single-layer prefiltering results with multilayer prefiltering results. For the first two rows, we also show the comparison with negative light assumed to delineate the ringing artifacts due to the lost frequencies.

simulated with a 50mm f/1.8 lens with object at a distance 100cm, and the camera focuses at 84cm; the separation between layers is 3.4cm. By comparing with the blurred images, clearly the perceived images preprocessed with the prefiltering algorithms are sharper. For the first two examples, we show both the negative light simulation and the real perceived images. The negative light simulation enables us to see more clearly how the ringing artifacts are successfully removed with multilayer prefiltering. In the meantime, the image contrast are greatly improved, as shown in the third row. On the right of Figure 4, the corresponding prefiltered layer images are shown.

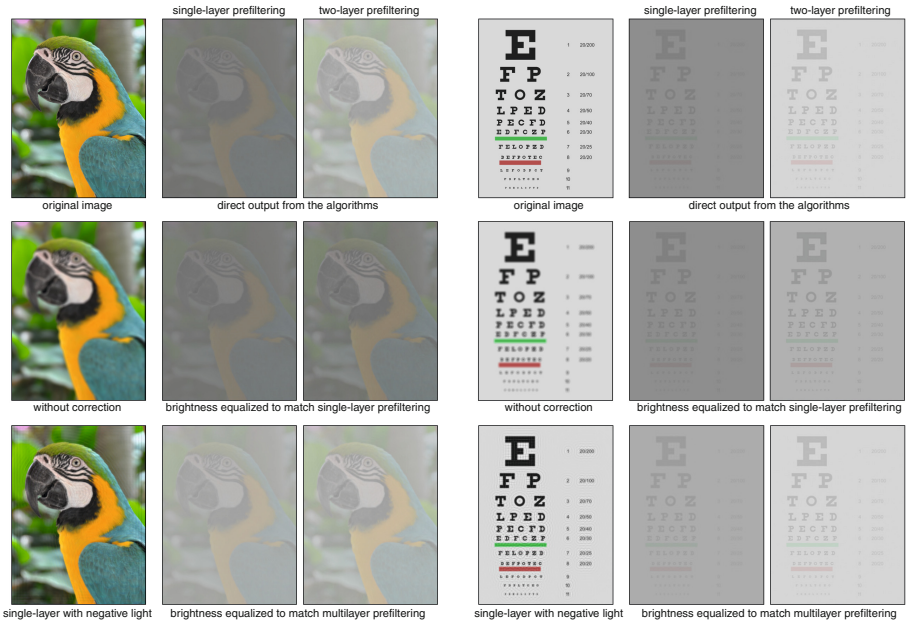

Fig. 5. Comparing simulated results when brightness are equalized. For a fair comparison, the brightness of the results from single-layer and multilayer prefiltering are equalized to match with each other. On the bottom left of each example, we manifest the ringing artifacts from single-layer prefiltering with negative light assumed.

Comparisons with equal brightness. As one might argue that the brightness setting (dynamic range) of the multilayer display may be different from a conventional display used for single-layer prefiltering, in Figure 5 we also show direct comparisons when the brightnesses are equalized to match each other. With the Michaelson contrast, which is defined as $(I_{max} - I_{min})/(I_{max} + I_{min})$, as our evaluation metric, the perceived image contrast is thus "independent" of display brightness. In both examples, the multilayer prefiltering results are still better than the single-layer prefiltering results in the image contrast, and as discussed

in Section 3.1, this is achieved by avoiding the zero-valued/weak spatial frequencies and greedy contrast optimization. On the bottom left of Figure 5, we also show the ringing artifacts in the single-layer prefiltering due to the zero-valued spatial frequencies and the weak frequencies affected by the regularization. These problems are eliminated by inverting the "all-pass-kernel" of the multilayer prefiltering algorithm.

Figure 6 summarizes experimental results achieved with the multilayer LCD. A digital camera was separated by 100 cm from the front layer of the prototype and focused at 16cm in front of the display, with the minimum f-number setting of f/1.8, resulting in an aperture diameter of 2.8cm. Figure 6 confirms the predicted contrast enhancement and elimination of ringing artifacts. For example, the inset region of the bird appears brighter and with higher contrast using multilayer prefiltering, rather than the prior single-layer prefiltering algorithm. Also note that the outline of the eye and the black stripes appear with less distortion using multilayer prefiltering. Ringing artifacts, visible on the left-hand side of the face of the blue toy, are eliminated.

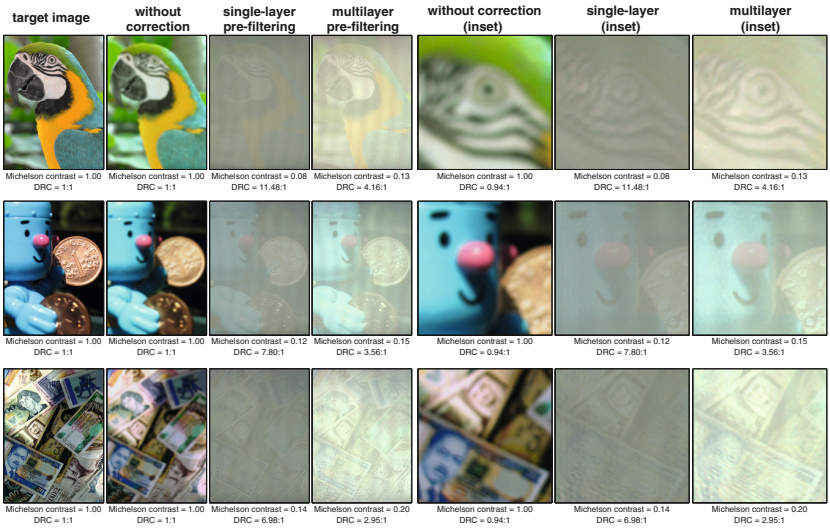

Fig. 6. Camera photographs of prefiltering results. Multilayer (two-layer) prefiltering improves image contrast. Remaining ringing artifacts are due to the spatially varying point spread function, spherical aberration, non-circular camera aperture, and offsets due to the non-linear gamma correction and diffraction.

Experimental results also reveal limitations of the linear spatially invariant (LSI) model. First, the medical display panels used in the prototype do not produce a linear radiometric response; gamma compression was applied to the displayed images, with a calibrated gamma value 2.2, to approximate a radiometrically linear display. Remaining radiometric non-linearities contribute

to ringing artifacts in the experimental imagery. Second, the lens produces a spatially-varying PSF, as analyzed by Kee et al. [9]; as seen in the bottom left of the currency image, differences between the modeled and experimental PSFs result in ringing artifacts in the periphery. However, the central region is well approximated by the defocused camera model. The camera lens aperture, consisting of several blades, does not produce a circular point spread function, and thus the optical transfer functions are different. Finally, the camera lens has some spherical aberration, which is not modeled in the current experiments.

We quantitatively assess the received image using the Michelson contrast metric, given by the ratio of the difference of the maximum and minimum values, divided by their sum. Michelson contrast is increased by an average of 44% using multilayer prefiltering rather than single-layer prefiltering. Prefiltering expands the dynamic range both above and below the range of radiance values that are physically supported by the display. We quantify this effect by evaluating the dynamic range compression (DRC) of the prefiltered images, given by the difference of the maximum and minimum values before normalization. By convention, the displayed normalized images always have a dynamic range of unity. For these examples, the dynamic range is reduced by an average of 42%, enabling contrast to be enhanced with multilayer prefiltering, despite normalization.

3.4 Discussion

In this work, we have optimized the Michaelson contrast and the dynamic range of the received image, as measured in a linear radiometric domain. A promising direction for future work is to explore alternative, possibly non-linear, perceptual optimization metrics. Following Grosse et al. [4], incorporating the human contrast sensitivity function (CSF) [8] may allow further perceived gains in contrast.

As established by theory and experiment, multilayer prefiltering achieves our primary goal: mitigating contrast loss and eliminating ringing artifacts observed with single-layer prefiltering. Yet, multilayer prefiltering comes at a cost of added components, increased computational complexity, and expanded display thickness. However, to our knowledge, our introduction of the multilayer partition function is the first avenue to allow demonstrable increases in the contrast of images presented with prefiltered displays.

4 Light Field Displays

Multilayer displays have previously been proposed as compressive light field displays [12,13]. These displays as well as Huang et al.'s [6] proposal to use them for vision correction all use some form of optimization to compute the optimal—in a least-squared error sense—pixel states for the problem at hand. An alternative implementation using conventional parallax barrier or microlens-based light field displays was recently proposed as well [7]. Although any of these display architectures can be used for the application of vision correction,

Huang et al [7] showed that even these simple light field displays, when driven by appropriate prefiltering algorithms, achieve superior contrast and resolution compared to all other implementations.

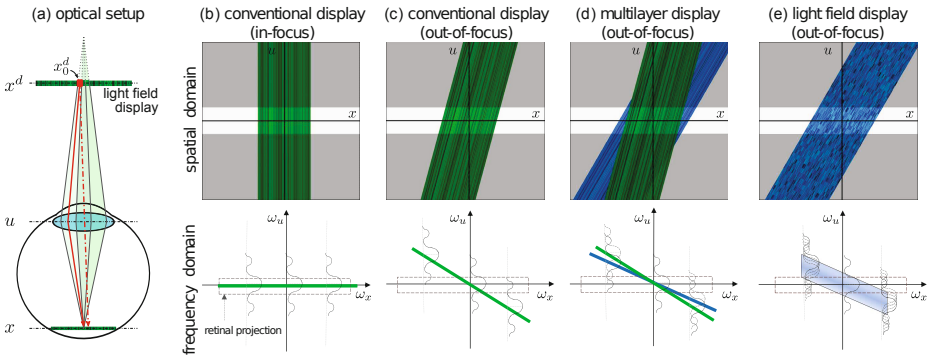

Fig. 7. Light field analysis for different displays. The light field emitted by a display is parameterized by its coordinates on the screen x^d, on the pupil u, and on the retina x (a). This light field propagates through the pupil and is projected into a 2D image on the retina. For an in-focus display, the light field incident on the retina is a horizontal line in the frequency domain (b). For a displayed image outside the accommodation range of the observer, the corresponding light field is slanted and energy is lost at some spatial frequencies (c). Multilayer displays utilize an additional display layer to preserve all spatial frequencies (d). With light field displays, frequency loss is also avoided; the perceived image frequencies are a combination of all spatio-angular frequencies of the incident light field (e). Each pixel on the screen (e.g., x_0^d) emits different intensities toward different regions on the pupil, allowing the same pixel to appear differently when observed from different locations on the retina (red arrows).

To understand how images are formed on the retina for an observed light field display, let us define the lateral position on the retina as x and that on the pupil as u (see Figure 7). Photoreceptors in the retina average over radiance incident from all angles; therefore, the perceived intensity $i\,(x)$ is modeled as:

$$i\,(x) = \int_{-\infty}^{\infty} l^d\,(\phi\,(x,u)\,,u)\,A\,(u)\,du, \tag{1}$$

where $\phi : \mathbb{R} \times \mathbb{R} \rightarrow \mathbb{R}$ is a mapping function that models refractions and aberrations in the eye from the spatio-angular coordinates inside the eye to a location on the screen, such that $x^d = \phi(x,u)$. The effect of the finite pupil diameter r is a multiplication of the light field with the pupil function $A\,(u) = rect\left(\frac{u}{r}\right)$. In the full 4D case, the *rect* function is replaced by a circular function modeling the shape of the pupil. In discrete form, Equation 1 becomes $\boldsymbol{i} = \mathbf{P}\boldsymbol{l}^d$.

The objective of an aberration-correcting display is to present a 4D light field to the observer, such that a desired 2D retinal projection is perceived. Assuming

that viewing distance, pupil size, and other parameters are known, the emitted light field can be found by optimizing the following objective function:

$$\begin{aligned} &\arg\min \boldsymbol{l}^d \ \|\boldsymbol{i} - \mathbf{P}\boldsymbol{l}^d\|_2 \\ &\text{subject to } 0 \leq l_i^d \leq 1, \quad \text{for } i = 1 \ldots N \end{aligned} \tag{2}$$

Here, $\boldsymbol{i}$ is the target image (given in normalized power per unit area) and the constraints of the objective account for physically feasible pixel states of the screen. Equation 2 can be solved using standard non-negative linear solvers. Equation 2 is an ill-posed problem for conventional 2D displays. The problem becomes invertible through the use of 4D light field displays.

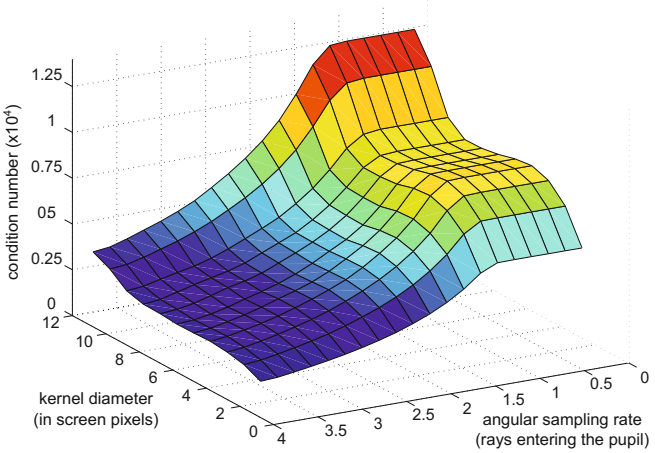

Fig. 8. The light field projection matrix corresponding to a defocused eye is ill-conditioned, implying that vision correction cannot be successful. With more angular resolution available in the emitted light field, more degrees of freedom are added to the system, resulting in lower condition numbers (lower is better), thereby making vision correcting at a high quality feasible. Even as few as 1.5 angular light field samples entering the pupil of an observer decrease the condition number.

To validate this argument, the condition number of the light field projection matrix $\mathbf{P}$ can be analyzed. Figure 8 shows the matrix conditioning for varying amounts of defocus and angular light field resolution (lower condition number is better). Increasing the angular resolution of the light field passing through the observer's pupil significantly decreases the condition number of the projection matrix for all amounts of defocus. This experiment demonstrates that the invertibility of Equation 2 is significantly increased (i.e. condition number is decreased) when multiple light rays emitted by the same location on the display surface enter the pupil. Only in this case is the problem of correcting refractive errors actually feasible to be solved.

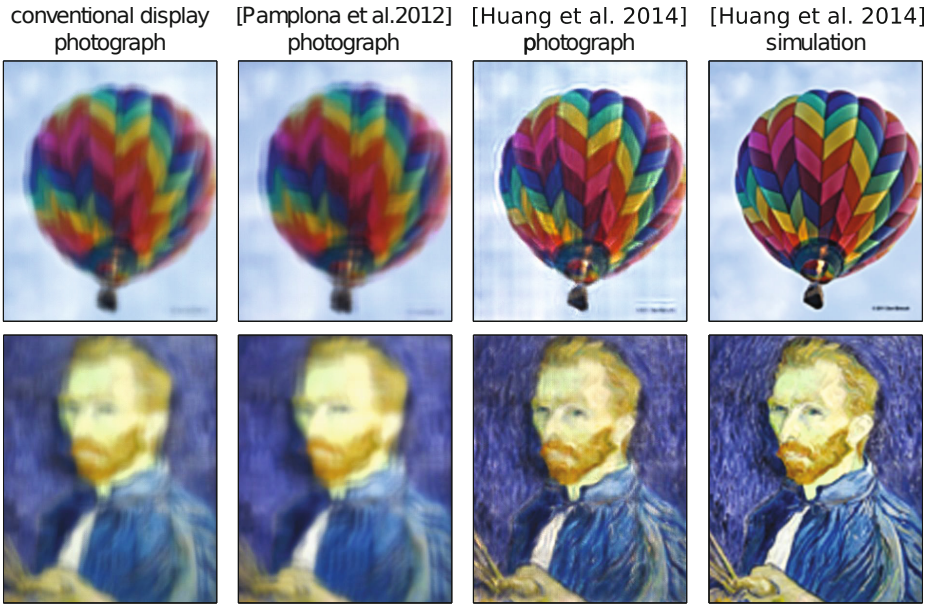

Fig. 9. Images shown on a conventional screen are blurred (first column). While direct light field display theoretically facilitates increased image sharpness (second column), achievable resolution is fundamentally limited by the spatio-angular resolution tradeoff of the required light field display. Light field prefiltering allows for significantly increased resolutions (third column). (From top, source images courtesy of dfbphotos (flickr), Vincent van Gogh, Houang Stephane (flickr), JFXie (flickr), Jameziecakes (flickr), Paul Cezanne, Pablo Picasso, Henri Matisse)

Figure 9 shows results captured with a pre-filtered light field display prototype (center right column). Photographs are captured with a camera equipped with a 50 mm lens at f/8. The display is placed at a distance of 25 cm to the camera. The camera is focused at 38 cm, placing the screen 13 cm away from the focal plane. This camera closely resembles a -6D hyperopic human eye. The results captured from the prototype (Figure 9, third column) closely resemble these simulations but contain minor artifacts that are due to moiré between the barrier mask and the display pixels. Compared to conventional 2D images shown on the screen (Figure 9, first column), image sharpness is significantly improved without requiring the observer to wear glasses. We also compare our approach to the method proposed by Pamplona et al. [11] for the same display resolution and spatio-angular tradeoff (Figure 9, second column). Basically, their approach uses the same display setup as ours but a direct solution rather than the proposed prefilter. Light field prefiltering outperforms the direct solution and allows for significantly increased resolution.

The quality achieved with all discussed vision-correcting display technologies is evaluated in Figure 10. A 10 inch tablet with a 300 PPI panel is simulated for this experiment; for the light field display approaches, a pinhole-based parallax

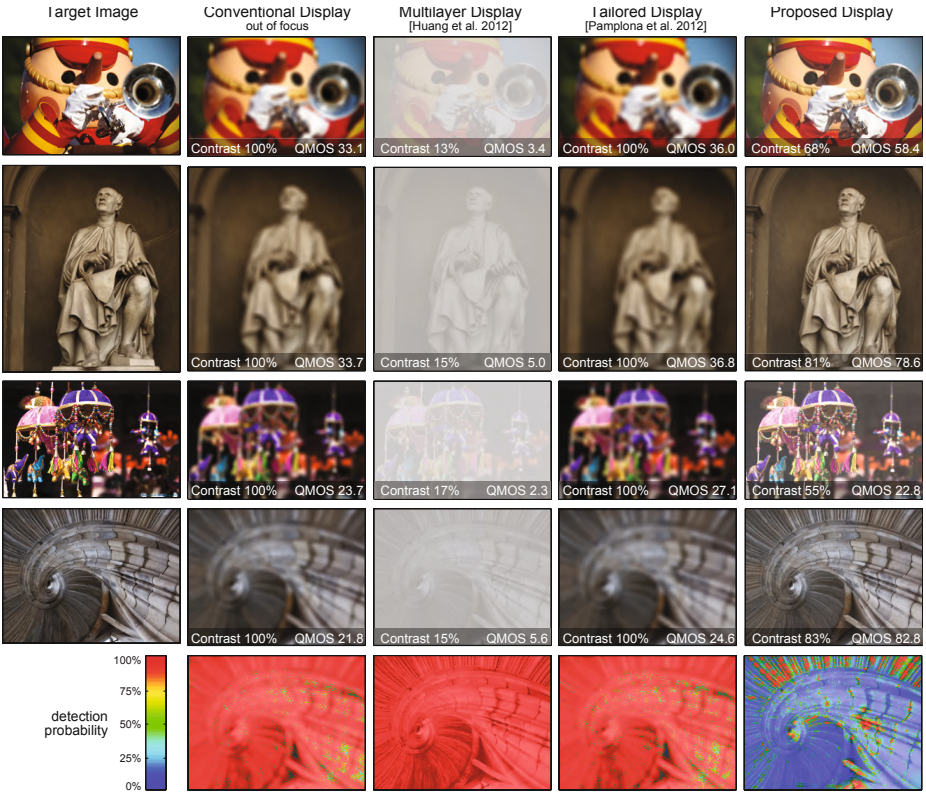

Fig. 10. Evaluation of vision-correcting displays. We compare simulations both qualitatively and quantitatively using contrast and quality-mean-opinion-square (QMOS) error metrics. A conventional out-of-focus display always appears blurred (second column). Multilayer displays with prefiltering improve image sharpness but at a much lower contrast (third column). Light field displays without prefiltering require high angular resolutions, hence provide a low spatial resolution (fourth column). The proposed method combines prefiltering and light field display to optimize image contrast and sharpness (right column). The QMOS error metric is a perceptually linear metric, predicting perceived quality for a human observer. We also plot maps that illustrate the probability of an observer detecting the difference of a displayed image to the target image (bottom row). Our method performs best in most cases. (Source images courtesy of flickr users Jameziecakes, KarHan Tan, Mostaque Chowdhury, Thomas Quine (from top))

barrier with 6.5 mm offset is simulated. The tablet is held at a distance of 30 cm and viewed with a -6.75D hyperopic eye; images are shown on the center of the display in a 10.8 cm $\times$ 10.8 cm area. Target contrast for prefiltering methods is manually adjusted to achieve the best PSNR for each example.

5 Conclusions

This is the first work to demonstrate focusing at more than one plane; although the eye has its natural focus plane, the device plane is also capable of generating a sharp image on the retina or the camera sensor. This is useful for heads-up-displays (HUDs), projecting useful information onto cars or objects when the windshield or Google glasses are close to the observer.

The near-field display is also useful in some real world applications, where wearing double glasses is cumbersome; the vision correcting display accomplishes two tasks with one device. There are some potential future directions that might engender interesting research, such as the vergences and the convergences problem of the eye when accommodating 3D content for entertainment applications.

Since some visual impairments involve high order optical aberrations, which are impossible to correct with eyeglasses unless gaze direction is restricted to be fixed, this work could improve the quality of life for people suffering from these ocular conditions. In this work, we show a promising framework for correcting higher order aberrations using a computational light field display approach; we fundamentally avoid the problem of making irregular-shaped optical elements. Through simulation, we demonstrate that the proposed prefiltering algorithm successfully compensates for different terms of the Zernike polynomials in the wavefront aberrations; however, physical experiments still need to be performed. In addition, it is unclear how the projection system behaves theoretically, and how the hardware works in practical uses.

For future work, we anticipate the condition analysis for the higher order aberrations would reveal insights on the hardware construction. We also expect higher order aberrations could have a potential impact on the off-axis viewing optimization.

Acknowledgments. This research was supported in part by the National Science Foundation at the University of California, Berkeley under grant number IIS-1219241, "Individualized Inverse-Blurring and Aberration Compensated Displays for Personalized Vision Correction with Applications for Mobile Devices."

References

1. Akeley, K., Watt, S.J., Girshick, A.R., Banks, M.S.: A stereo display prototype with multiple focal distances. ACM Trans. Graph. **23**(3), 804–813 (2004). http://doi.acm.org/10.1145/1015706.1015804
2. Alonso Jr, M., Barreto, A.B.: Pre-compensation for high-order aberrations of the human eye using on-screen image deconvolution. IEEE Engineering in Medicine and Biology Society. **1**, 556–559 (2003)
3. Archand, P., Pite, E., Guillemet, H., Trocme, L.: Systems and methods for rendering a display to compensate for a viewer's visual impairment. International Patent Application PCT/US2011/039993 (2011)
4. Grosse, M., Wetzstein, G., Grundhöfer, A., Bimber, O.: Coded aperture projection. ACM Trans. Graph. (2010). http://doi.acm.org/10.1145/1805964.1805966

5. Huang, F.C., Barsky, B.A.: A framework for aberration compensated displays. Tech. Rep. UCB/EECS-2011-162, EECS Department, University of California, Berkeley, December 2011. http://www.eecs.berkeley.edu/Pubs/TechRpts/2011/EECS-2011-162.html
6. Huang, F.C., Lanman, D., Barsky, B.A., Raskar, R.: Correcting for optical aberrations using multilayer displays. ACM Trans. Graph. **31**(6), 185:1–185:12 (2012). http://doi.acm.org/10.1145/2366145.2366204
7. Huang, F.C., Wetzstein, G., Barsky, B.A., Raskar, R.: Eyeglasses-free display: Towards correcting visual aberrations with computational light field displays. ACM Transaction on Graphics xx, 0 August 2014. http://graphics.berkeley.edu/papers/Huang-EFD-2014-08/
8. Kaufman, P., Alm, A.: Adler's Physiology of the Eye (Tenth Edition). Mosby (2002)
9. Kee, E., Paris, S., Chen, S., Wang, J.: Modeling and removing spatially-varying optical blur. In: IEEE International Conference on Computational Photography (2011)
10. Lanman, D., Wetzstein, G., Hirsch, M., Heidrich, W., Raskar, R.: Polarization fields: dynamic light field display using multi-layer LCDs. ACM Trans. Graph. 30(6) (2011). http://doi.acm.org/10.1145/2070781.2024220
11. Pamplona, V.F., Oliveira, M.M., Aliaga, D.G., Raskar, R.: Tailored displays to compensate for visual aberrations. ACM Trans. Graph. **31**(4), 81:1–81:12 (2012). http://doi.acm.org/10.1145/2185520.2185577
12. Wetzstein, G., Lanman, D., Heidrich, W., Raskar, R.: Layered 3d: Tomographic image synthesis for attenuation-based light field and high dynamic range displays. ACM Trans. Graph. (SIGGRAPH) **30**(4), 95:1–95:12 (2011)
13. Wetzstein, G., Lanman, D., Hirsch, M., Raskar, R.: Tensor displays: Compressive light field synthesis using multilayer displays with directional backlighting. ACM Trans. Graph. (SIGGRAPH) **31**(4), 80:1–80:11 (2012)
14. Yellott, J.I., Yellott, J.W.: Correcting spurious resolution in defocused images. Proc. SPIE 6492 (2007)